Available online at www.sciencedirect.com
ScienceDirect
Trans. Nonferrous Met. Soc. China 34(2024) 4085−4098
Transactions of Nonferrous Metals Society of China
www.tnmsc.cn

Effects of monosaccharides and protein in extracellular polymeric substances of *Klebsiella aerogenes* on crystalline forms of $CaCO_3$ crystals

Nan HU[1], Ai-shu LI[1,2], Huang YU[1], Yu-long LIU[1], Hui ZHANG[1], Zhi-hui YANG[2], Guang-yue LI[1], De-xin DING[1]

1. Key Discipline Laboratory for National Defence of Biotechnology in Uranium Mining and Hydrometallurgy, University of South China, Hengyang 421001, China;
2. School of Metallurgy and Environment, Central South University, Changsha 410083, China

Received 3 December 2023; accepted 7 August 2024

Abstract: A strain of *Klebsiella aerogenes* (*K. aerogenes*) capable of decomposing calcium acetate for $CaCO_3$ biomineralization was screened, and the optimum conditions for producing the maximum mass of $CaCO_3$ crystals induced by *Klebsiella aerogenes* were found to be 0.25 mol/L calcium acetate, 4% inoculum level, and pH 7. Following that, the monosaccharides and proteins contained in the extracellular polymeric substances (EPS) of *Klebsiella aerogenes* were identified. The effects of additional identified monosaccharide and proteins on the crystalline form conversion of $CaCO_3$ crystals were investigated, and the additional monosaccharides were found to promote the crystalline form conversion of $CaCO_3$ crystals from vaterite to calcite. Specifically, adding 1.00 g/L glucuronic acid was observed to enhance the conversion of crystalline phases of $CaCO_3$ crystals to calcite completely after 5 d. Meanwhile, additional catalase was observed to contribute to the regular morphology of $CaCO_3$ crystals without affecting their crystalline phases. The results indicate that the additional glucuronic acid influences the crystalline forms of $CaCO_3$ crystals significantly.

Key words: uranium; $CaCO_3$ crystal; microbially induced $CaCO_3$ precipitation; extracellular polymeric substances; *Klebsiella aerogenes*

1 Introduction

Uranium tailings repository is widely acknowledged as the main source of radioactive pollution in the nuclear industry. The release, transportation, and entry of heavy metals and radionuclides into food chains can significantly endanger human health [1,2]. Therefore, there is an urgent demand for developing new technologies to deal with the pollution of uranium tailings repository. Remediation technologies for uranium pollution mainly include physical, chemical, and biological methods. Bioremediation stands out due to its low cost, easy operation, and low environmental disturbance, offering an eco-friendly, cost-effective, and in-situ remediation strategy for uranium contamination [3]. Microbially induced calcite precipitation (MICP) remediates pollutants in the environment through biomineralization, which is environmentally friendly and adaptable [4]. Thus, MICP is considered as a prospective green bioremediation method for addressing uranium pollution in the environment.

MICP can occur in a variety of microbial metabolic activities, such as urea hydrolysis, photosynthesis, denitrification, and sulfidation reactions [5−8]. Studies have shown that urea hydrolysis and sulfidation typically produce secondary pollutants, such as NH_4^+ and H_2S [9,10].

Corresponding author: De-xin DING, Tel: +86-13974753170, E-mail: dingdexinusc@163.com
DOI: 10.1016/S1003-6326(24)66660-4

Although both photosynthesis and denitrification are environmentally friendly, they have drawbacks because photosynthesis is mainly realized by algae while denitrification is influenced by carbon sources [11,12]. It has been found that bacteria can produce $CaCO_3$ crystals by decomposing calcium acetate and producing CO_2 and H_2O, which prevents secondary pollution to the surrounding environment. Therefore, it is particularly important to screen a carbonate mineralizing strain of decomposing calcium acetate, without generating secondary pollution [13].

Certainly, bacteria induce the formation of various crystalline phases of $CaCO_3$ crystals, including calcite, aragonite, and vaterite [14]. The thermodynamic stability of $CaCO_3$ crystals produced by MICP is closely related to the crystalline phases of $CaCO_3$ crystals. Calcite has the highest thermodynamic stability, which could contribute to enhancing the mechanical properties of solidified samples [15,16]. Therefore, enhancing the crystalline phase conversion of $CaCO_3$ crystals to calcite may be the key technique to improve the MICP. Previous research has shown that biomolecules such as monosaccharides and proteins in bacterial extracellular polymeric substances (EPS) can affect the growth and morphology of $CaCO_3$. WU and ZENG [17] showed that the growth of crystalline facets into calcite could be regulated by using alginate. KAYANO et al [18] concluded that in vitro coccolith polysaccharides elongated calcite crystals in the *c* axis. AZULAY et al [19] found that two bacterial ECM proteins of TasA and TapA and an exopolysaccharide induced the formation of complex $CaCO_3$ structures. Therefore, understanding the mechanism of how monosaccharides and proteins promote the conversion of $CaCO_3$ crystals to calcite could be an important contribution to future MICP applications.

In this work, a strain of *Klebsiella aerogenes* (*K. aerogenes*) that can decompose calcium acetate was screened, and the effects of its monosaccharides and proteins in the extracellular polymeric substances on the crystalline phases and morphology of $CaCO_3$ crystals were explored. In this study, the additional glucuronic acid was found to influence the crystalline forms of $CaCO_3$ crystals significantly. This study aims to investigate the mechanisms of regulating the crystalline forms of $CaCO_3$ crystals by monosaccharides and proteins produced by *K. aerogenes*, and provide a theoretical framework for enhancing the crystalline form conversion of $CaCO_3$ crystals and a green strategy for dealing with the pollution of uranium tailings repository.

2 Experimental

2.1 Bacterial isolation, identification and culture

K. aerogenes was isolated from the soil at the University of South China (112°N, 26°E), and the results of strain identification are shown in Fig. S1 and Table S1 of supporting information (SI). The strain was cultured in 100 mL sodium acetate liquid medium (pH=7.0) with 20.00 g/L sodium acetate and 4.00 g/L yeast extract. It has been found that the strain is capable of producing $CaCO_3$ crystals by decomposing calcium acetate, with only CO_2 and H_2O as by-products, posing no risk of secondary pollution to the environment.

The strain was identified by 16S rDNA sequencing, which was entrusted to Sangon Biotech (Shanghai) Co., Ltd. According to the results of the 16S rDNA gene sequence analysis, the strain showed the highest degree of similarity (100%) with *K. aerogenes*. It has been preserved at the Chinese Centre for the Preservation of Typical Microorganisms (Wuhan) with the collection number *K. aerogenes* 11027. The bacterial sequence has been uploaded to GenBank and the accession number is ON139648.

2.2 Effects of pH, bacterial inoculum, and calcium acetate on mass of $CaCO_3$ crystals

To investigate the effects of pH, bacterial inoculum amount, and concentration of calcium acetate on the mass of $CaCO_3$ crystals, experiments were conducted at different pH values (pH 3, 5, 7 and 9), bacterial inoculum amounts (1%, 2%, 4% and 6%) and calcium acetate concentrations (0.05, 0.10, 0.25 and 0.50 mol/L). The bacteria solution was inoculated into the 100 mL of calcium acetate culture medium (17.50 g/L calcium acetate, 4.00 g/L yeast extract and pH 7) and incubated in the shaking incubator at 100 r/min and 30 °C for 11 d. At the end of culture, all the liquid in the conical flask was transferred to a 50 mL centrifuge tube, centrifuged at 8000 r/min for 10 min, the

supernatant was filtered, and the precipitate was dried at 60 °C.

2.3 Extraction of extracellular polymeric substance of *K. aerogenes*

The extracellular polymeric substances (EPS) of *K. aerogenes* was extracted using a cation exchange resin method [20,21]. Bacterial cells were collected through centrifugation at 8000 r/min and 4 °C for 15 min using a high-speed freezing centrifuge. Subsequently, bacteria cells were suspended in 100 mL deionized water, sonicated at 100 W for 2 min, and then mixed with 20.00 g 732 cation exchange resin (CER, Sinopharm Group). The bacterial fluid and resin were agitated at 4 °C for 9 h. The bound EPS was separated by centrifugation at 10000 r/min for 10 min at 4 °C. The EPS solution was filtered by a hydrophobic polyether sulfone (PES) membrane with a pore size of 0.22 μm, and freeze-dried to obtain pure EPS solid, which was stored at −80 °C for subsequent analysis.

2.4 Determination of monosaccharide components of EPS

Monosaccharides from the hydrolyzed polysaccharides in the EPS were analyzed using a previously modified method [22]. The types and concentrations of these monosaccharides of the EPS were determined through the high performance liquid chromatography (HPLC). Samples were weighed in a hydrolysis tube and standard solutions with different concentrations of monosaccharides (mannose, ribose, rhamnose, glucuronic acid, galacturonic acid, glucose, galactose, xylose, arabinose, and fucose) were prepared. The monosaccharides were determined under the following conditions: a reversed-phase C18 column (Agilent 4.6 mm × 250 mm × 5 μm); the flow rate, column temperature, detection wavelength, and injection volume were 1 mL/min, 25 °C, 245 nm and 10 μL, respectively. Mobile phase A was 82% ultrapure water with 0.1 mol/L KH_2PO_4 and mobile phase B was 18% acetonitrile.

2.5 Determination of protein components of EPS

To determine the components of proteins of EPS, proteins were extracted using a slightly modified method [23]. EPS was dissolved in urea and Tris, and reduced with DTT and alkylated with iodoacetamide at room temperature in the dark. Then, 3 μg trypsin (Promega) was added in 50 mmol/L NH_4HCO_3 (overnight at 37 °C). The peptide content was estimated by UV light spectral density at 280 nm, using an extinction coefficient of 1.1 of 0.1% solution that was calculated on the basis of the frequency of tryptophan and tyrosine in vertebrate protein. Then, liquid chromatography-mass spectrometry (LC-MS) technique was used for mass spectrometric characterization of the proteins of EPS. Triplicates of LC-MS analysis were performed in each sample.

2.6 Effects of monosaccharides and protein on crystalline form of $CaCO_3$ crystals

K. aerogenes was cultured for 24 h in the sodium acetate culture medium (20.00 g/L sodium acetate, 4.00 g/L yeast extract, pH 7) under stirring at 100 r/min and 30 °C. Subsequently, 1 mL of the bacterial suspension was inoculated into 100 mL calcium acetate medium (17.50 g/L calcium acetate, 4.00 g/L yeast extract, pH 7) and cultured under stirring at 100 r/min and 30 °C. After incubation for 3 d, the additional monosaccharides and protein including glucose, mannose, glucuronic acid, mixed monosaccharides (glucose, mannose and glucuronic acid), and catalase solutions (the final concentrations of each monosaccharide and catalase were 1.00 g/L and 50.00 mg/L, respectively) were added to the calcium acetate medium, respectively. Finally, the solution was incubated for 5 d, collected and put into a 50 mL centrifuge tube, shaking at 8000 r/min for 10 min. The $CaCO_3$ crystals were dried at 60 °C for 48 h after discarding the supernatant solution.

The crystalline phases of $CaCO_3$ crystals were analyzed by X-ray diffraction (D8 Advance, Germany), the morphological changes of the $CaCO_3$ crystals were observed with a scanning electron microscope (SEM) (Sigma 300, Germany), and the charge property and functional groups in $CaCO_3$ crystals were tested with a zeta potential analyzer (Nano ZS90, UK) and a Fourier transform infrared spectrometer (FTIR) (IRAffinity 1S, Japan). The morphology, crystal information, and elemental distribution of $CaCO_3$ crystals were tested by transmission electron microscopy (TEM) (Talos F200X G2, Thermo Fisher Scientific).

2.7 Statistical analysis

Data were presented as the mean values of three replicates, and the standard deviations were used to analyze the experimental data. Particle size distribution of the $CaCO_3$ crystals was measured using Image J software based on the SEM images. The XRD patterns were analyzed by Jade 6.0 software. The patterns were performed using Origin 2021.

3 Results and discussion

3.1 Effects of bacterial culture conditions on mass of $CaCO_3$ crystals

The effects of initial pH value, bacterial inoculum amount, and calcium acetate concentration on the mass of $CaCO_3$ crystals are shown in Fig. 1. The mass of $CaCO_3$ crystals increases with the cultivation time until 9 d. Figure 1(a) shows that the mass of $CaCO_3$ crystals is significantly affected by the initial pH value. The maximum mass of $CaCO_3$ crystals is 0.84 g at pH 7. Both low and high pH values affect the growth and metabolism of *K. aerogenes*, leading to a decrease in the mass of $CaCO_3$ crystals. Figure 1(b) shows that the bacterial inoculum amount has little influence on the mass of $CaCO_3$ crystals. The maximum mass of $CaCO_3$ crystals is 0.96 g when the bacterial inoculum amount is 4%. Figure 1(c) shows that the mass of $CaCO_3$ crystals is significantly affected by the concentration of calcium acetate, and the maximum mass of $CaCO_3$ crystals is 1.23 g when the calcium acetate concentration is 0.25 mol/L. Calcium acetate serves as nutrient and calcium source at the same time, leading to an enhancement in the mass of $CaCO_3$ crystals. However, high concentration of calcium acetate is observed to decrease the mass of $CaCO_3$ crystals, possibly due to the alteration of Ca^{2+} concentration affecting pressure balance and reducing enzyme activity during bacterial metabolism [24]. The initial low mass of $CaCO_3$ crystals is attributed to bacterial adaptation to the calcium acetate medium. Subsequently, there is a decrease in the mass of $CaCO_3$ crystals after 9 d, possibly due to the decrease of bacterial metabolic activity. Taken together, the results demonstrate that the optimum conditions for $CaCO_3$ crystals induced by *K. aerogenes* are found to be 0.25 mol/L calcium acetate, 4% bacterial inoculum amount, and pH 7.

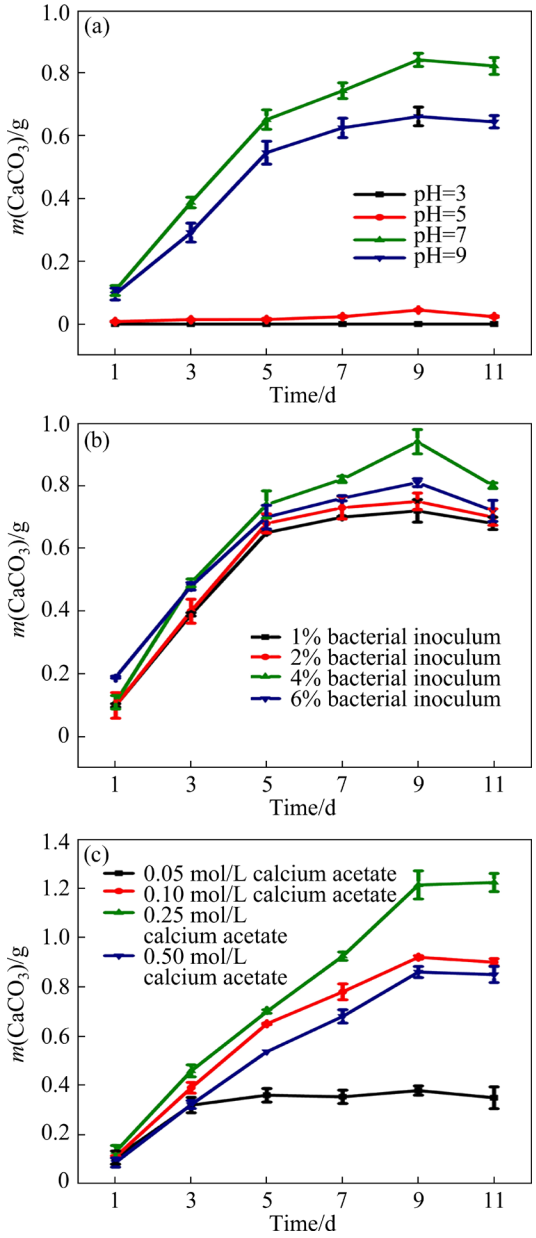

Fig. 1 Effects of bacterial culture conditions on mass of $CaCO_3$ crystals: (a) pH; (b) Bacterial inoculum amount; (c) Concentration of calcium acetate

3.2 Identification of monosaccharide and protein components of EPS

Monosaccharides from the hydrolyzed polysaccharides in the EPS of *K. aerogenes* were analyzed by HPLC, and the total ion flow chromatogram is shown in Fig. 2. Mannose, ribose, glucuronic acid, galacturonic acid, glucose, and galactose are the main monosaccharide species in the EPS of *K. aerogenes.* Besides, the protein types identified by LC-MS analysis are shown in Table 1. The EPS of *K. aerogenes* mainly contains 570 types of proteins.

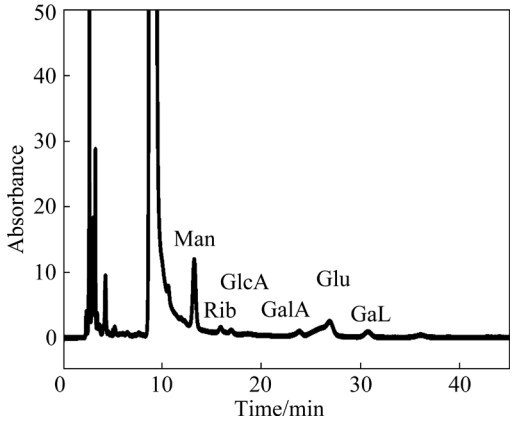

Fig. 2 Total ion flow chromatogram of monosaccharides in EPS (Man−Mannose; Rib−Ribose; GlcA−Glucuronic acid; GalA−Galacturonic acid; Glu−Glucose; Gal−Galactose)

To compare the effects of different monosaccharides on the crystalline forms of $CaCO_3$ crystals, mannose, glucose, and glucuronic acid were selected for subsequent experiments. In addition, catalase is easily accessible, widely distributed in organisms, and capable of entering $CaCO_3$ crystal [25]. Furthermore, the results show that EPS contains catalase, which has been widely reported to interact with $CaCO_3$ crystal [26]. Therefore, the addition of catalase during the biomineralization of *K. aerogenes* was considered.

3.3 Effects of monosaccharides and protein on crystalline phases and morphology of $CaCO_3$ crystals

3.3.1 Crystalline structure of $CaCO_3$ crystals

The crystalline structure of the $CaCO_3$ crystals was analyzed by XRD, and the XRD patterns of $CaCO_3$ crystals are shown in Figs. 3(a, b). The identified signature peaks of calcite at 2θ values of 23.03°, 29.37° and 35.94° are attributed to the (102),

Table 1 Protein components of EPS

Serial No.	Protein name	Number of protein kinds[a]	Score[b]	Sequence coverage[c]
1	Capsule assembly Wzi family protein	322	33.253	15
2	Elongation factor Tu	145	104.93	37.1
3	RND family efflux transporter MFP subunit	94	37.162	15.9
4	Malate dehydrogenase	85	43.084	17.4
5	Catalase-peroxidase (CP)	84	40.398	10.6
6	TonB-dependent receptor plug domain-containing protein	84	6.0910	11.9
7	Ribonuclease E	83	24.517	6
8	DNA-binding protein	80	48.384	63.3
9	Uncharacterized protein	78	40.048	18.9
10	Transaldolase B	73	49.091	32.5
11	TonB-dependent receptor	72	16.891	14.3
12	Catalase	69	17.66	6.4
13	ATP-dependent chaperone ClpB	66	27.943	9.1
14	Translation initiation factor IF-2	66	26.002	5.1
15	Phosphoglucomutase	64	18.967	11
16	Isoleucyl-tRNA synthetase	64	6.2463	10.8
17	Putative TonB-dependent receptor	62	5.9619	15.4
18	Succinate-semialdehyde dehydrogenase	61	6.0143	11.2
19	Aconitate hydratase	60	6.1804	12.4
20	Others	16799	10941.0025	11588
Total	570 [d]	18511	11425.5024	11933.9

a: Proteins with similar peptide segments, sequences, structures, functions, and values; b: Amino acids detected/total number of amino acids; c: Total number of sequences matched; d: 570 different types of proteins in EPS

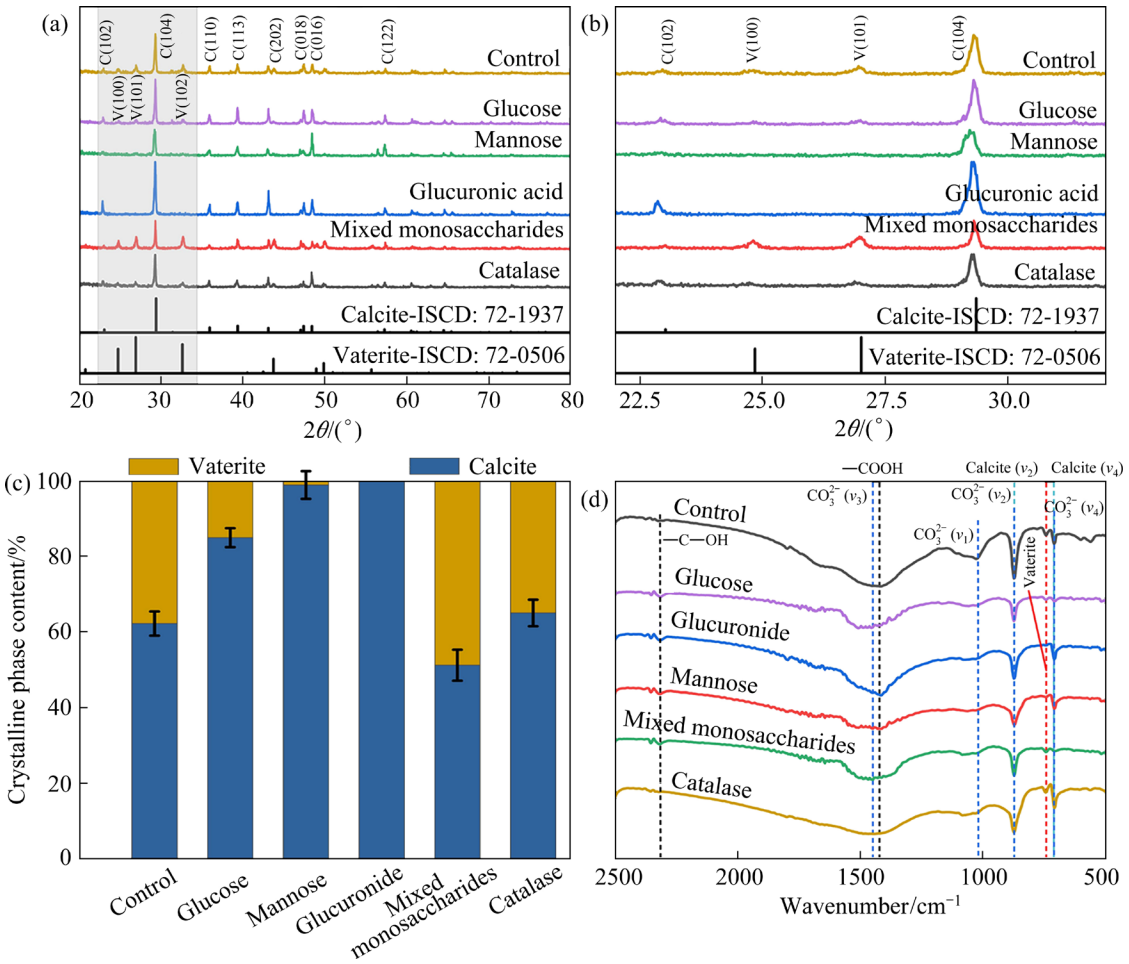

Fig. 3 Effects of monosaccharides and protein on crystalline structure, crystalline phase content and surface functional groups of $CaCO_3$ crystals: (a) XRD patterns (V=Vaterite, C=Calcite); (b) Enlarged view of shaded area of (a); (c) Crystalline phase content; (d) FTIR spectra

(104) and (110) planes, respectively. The identified signature peaks of vaterite at 2θ values of 24.87°, 27.03° and 32.17° are assigned to the (100), (101) and (102) planes, respectively. The crystalline phases from XRD data were analyzed by MDI Jade 6.0 (Fig. 3(c)). The results show significant differences in the crystalline phases of $CaCO_3$ crystals influenced by glucose, mannose, glucuronic acid, catalase, and mixed monosaccharides. The contents of calcite in the experimental groups are 84.9%, 98.8%, 100%, 51.2% and 65.0% (62.2% in the control group), respectively, indicating that glucose, mannose, and glucuronic acid could enhance the conversion of crystalline phases of $CaCO_3$ crystals to calcite, while catalase does not significantly affect the crystalline phase conversion of $CaCO_3$ crystals. It is noted that the mixed monosaccharides have an inhibitory effect on the crystalline phases, which might be related to the concentration of monosaccharide.

3.3.2 Effects of surface functional groups and zeta potential on $CaCO_3$ crystals

FTIR analysis was conducted to investigate the effects of surface functional groups on the $CaCO_3$ crystals (Fig. 3(d)). The infrared spectra of samples displayed distinct characteristic peaks of $CaCO_3$ crystals. Figure 3(d) shows that CO_3^{2-} has four IR absorption bands at 1570−1255 cm^{-1} (υ_3), 1090−1045 cm^{-1} (υ_1), 890−836 cm^{-1} (υ_2), and 760−675 cm^{-1} (υ_4), respectively [27]. Among these, the absorption peaks at 874 cm^{-1} (υ_2) and 713 cm^{-1} (υ_4) are characteristic of calcite [28]. Compared with the sample treated with glucuronic acid, an additional absorption peak at 744 cm^{-1} is observed in the sample treated with glucose, mannose, and catalase, indicating the presence of vaterite [27]. No obvious characteristic peak of vaterite is observed after adding glucuronic acid, suggesting a conversion of vaterite to calcite by the glucuronic acid. The addition of glucuronic acid results in a rightward

shift in the υ_3 absorption peak of the crystal at 1450 cm^{-1}, which is attributed to the stretching vibrations of carboxylate groups [29,30]. In the presence of monosaccharides, $CaCO_3$ crystals shows the absorption peak of C—OH bond of glycosylation products at 2000−2500 cm^{-1}. The addition of catalase increases the area of the absorption peak near υ_3, which could be attributed to the stretching vibrations by the benzene ring group at 1605 cm^{-1} [31]. These results indicate that adsorption occurs among $CaCO_3$ crystals, monosaccharides and protein. The zeta potentials of $CaCO_3$ in the presence of monosaccharides and protein are shown in Fig. S2 of SI, demonstrating a negative trend in the presence of glucose, mannose, glucuronic acid, and catalase. The results further demonstrate that hydroxyl and carboxyl groups with negative charge could be absorbed on the surface of $CaCO_3$ crystals.

3.3.3 Morphologies of $CaCO_3$ crystals

Scanning electron microscopy (SEM) was utilized to analyze the morphologies of $CaCO_3$ crystals in the presence of additional monosaccharides and protein, and the results are shown in Fig. 4. The control group samples (Figs. 4(a, b)) are composed of micron-sized calcite and vaterite, appearing as scattered and irregular particles. The morphology of $CaCO_3$ crystals in the presence of glucuronic acid (Figs. 4(c, d)) are distinctly different from the control group, exhibiting pure rhombic crystals, a typical structure of calcite. The addition of catalase results in the agglomeration of spherical $CaCO_3$ crystals particles (Figs. 4(e, f)), potentially influenced by electrostatic interactions. In the presence of glucose and mannose, the $CaCO_3$ crystals are composed of calcite and vaterite, with vaterite surrounding the calcite (Figs. 4(g–j)). Thus, it could be assumed that parts of calcite are formed by the dissolution and recrystallization of vaterite. Additionally, the addition of mixed monosaccharides results in numerous small $CaCO_3$ crystals particles with an average diameter of approximately 1 μm (Figs. 4(k, l)). Furthermore, the particle size distributions (PSDs) are presented in Fig. 5. The average particle size of control group samples is 8.99 μm (Fig. 5(a)), and samples treated with glucuronic acid, catalase, glucose, mannose and mixed monosaccharides have average particle sizes of 25.29 μm (Fig. 5(b)), 16.90 μm (Fig. 5(c)), 19.00 μm (Fig. 5(d)), 21.96 μm, (Fig. 5(e)), and 1.68 μm (Fig. 5(f)), respectively. The additional

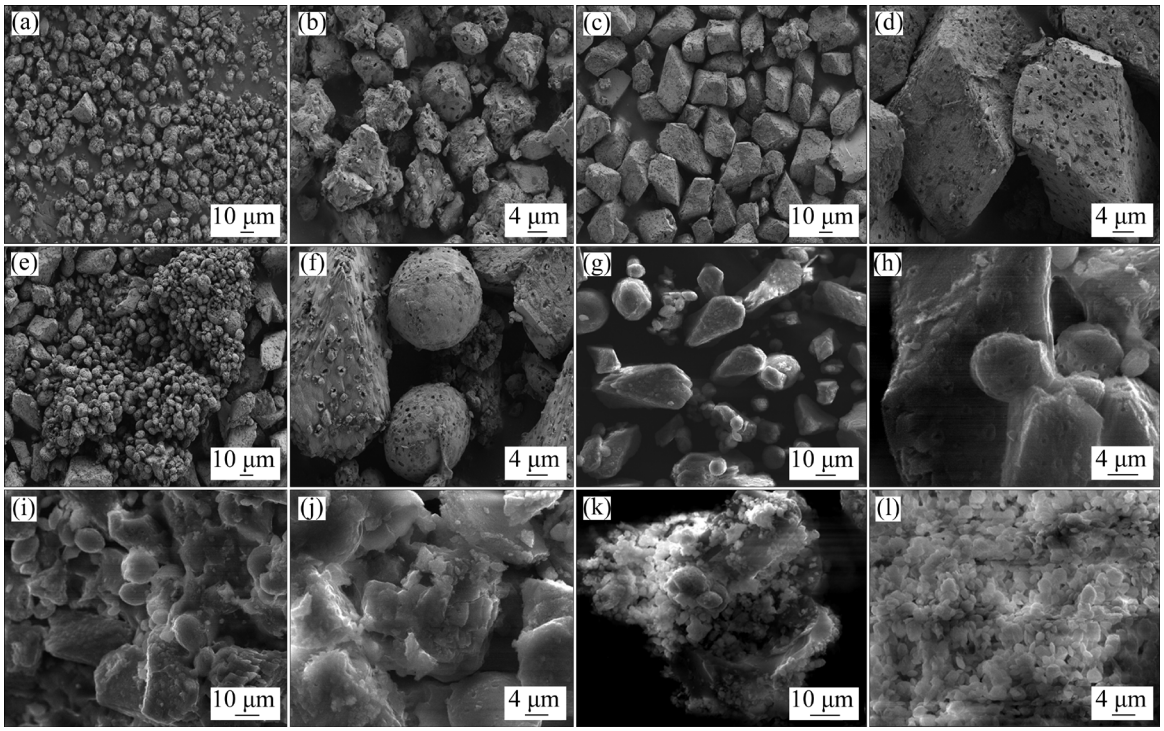

Fig. 4 Morphologies of $CaCO_3$ crystals in the presence of monosaccharides and protein: (a, b) Control group; (c, d) Glucuronic acid; (e, f) Catalase; (g, h) Glucose; (i, j) Mannose; (k, l) Mixed monosaccharides (glucose, mannose and glucuronic acid)

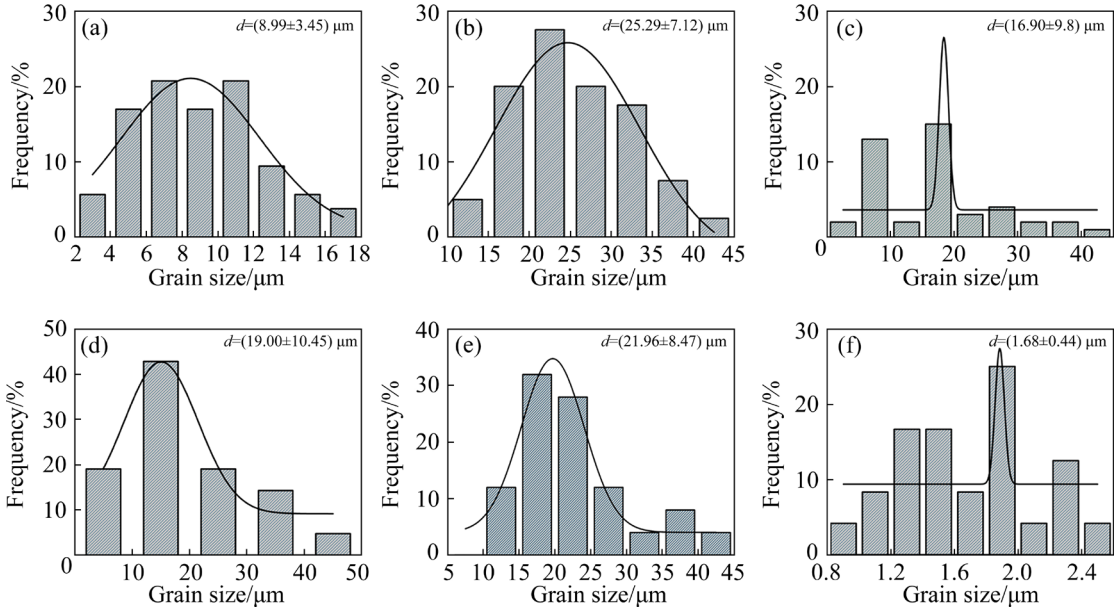

Fig. 5 Effects of monosaccharides and protein on particle size distribution of $CaCO_3$ crystals: (a) Control group; (b) Glucuronic acid; (c) Catalase; (d) Glucose; (e) Mannose; (f) Mixed monosaccharides (glucose, mannose and glucuronic acid)

monosaccharides and protein lead to an increase in crystal size, indicating that the monosaccharides and protein of *K. aerogenes* have accelerated the crystal nucleation. However, the additional mixture of glucose, mannose, and glucuronic acid decreases the average particle size of the crystals to 1.68 μm. Notably, visible bacterial imprints are observed on the surface of calcite and vaterite crystals, suggesting that *K. aerogenes* is involved in the mineralization process and could be used as nucleation sites for the growth and formation of $CaCO_3$ crystals [32,33].

3.3.4 Lattice spacing and distribution of elements of $CaCO_3$ crystals

To further reveal the mechanism for the formation of $CaCO_3$ crystals, high-resolution images were taken from selected areas, and lattice labeling was performed using Digital Micrograph software**.** The samples underwent thorough crushing and dispersion in ethyl alcohol via sonication for 20 min before TEM analysis. The results indicate that $CaCO_3$ crystals consist of aggregated nanosized subunits in the presence of glucose (Fig. 6(b)). It can be inferred that the mineralization of $CaCO_3$ is due to the accumulation of nano-particulate amorphous $CaCO_3$ (ACC), which is subsequently dehydrated and crystallized to the $CaCO_3$ nano-grains. The $CaCO_3$ crystals are shown to be shuttle-shaped in the presence of glucuronic acid (Fig. 6(d)). Meanwhile, in the presence of mixed monosaccharides, the $CaCO_3$ crystals show morphological characteristics of the three monosaccharides (Fig. 6(e)). Furthermore, the additional catalase contributes to the regular morphology of $CaCO_3$ crystals (Fig. 6(f)). The elemental distribution results for Ca, C, and O in the samples are shown in Figs. 6(g−l). Interestingly, the Ca content of $CaCO_3$ crystals decreases after the addition of monosaccharides compared to the catalase and control groups, owing to the reaction of hydroxyl and carboxyl groups of glucose, mannose, and glucuronic acid with Ca^{2+}, resulting in a decrease of the Ca content of the precipitates. However, the adsorption of catalase is solely related to the protein-crystal interaction but not to the reaction with Ca^{2+}. To reveal the mechanism for forming of the $CaCO_3$ crystals, some high-resolution images were taken from the selected areas, and lattice labeling was performed using Digital Micrograph software (Figs. 7(a−f)). It is observed that the crystal plane lattice spacing of calcite (104) is different under the influence of additional monosaccharides and protein. These results indicate that the additional monosaccharides and protein alter the lattice spacing of $CaCO_3$ crystals. Furthermore, the crystalline phases of $CaCO_3$

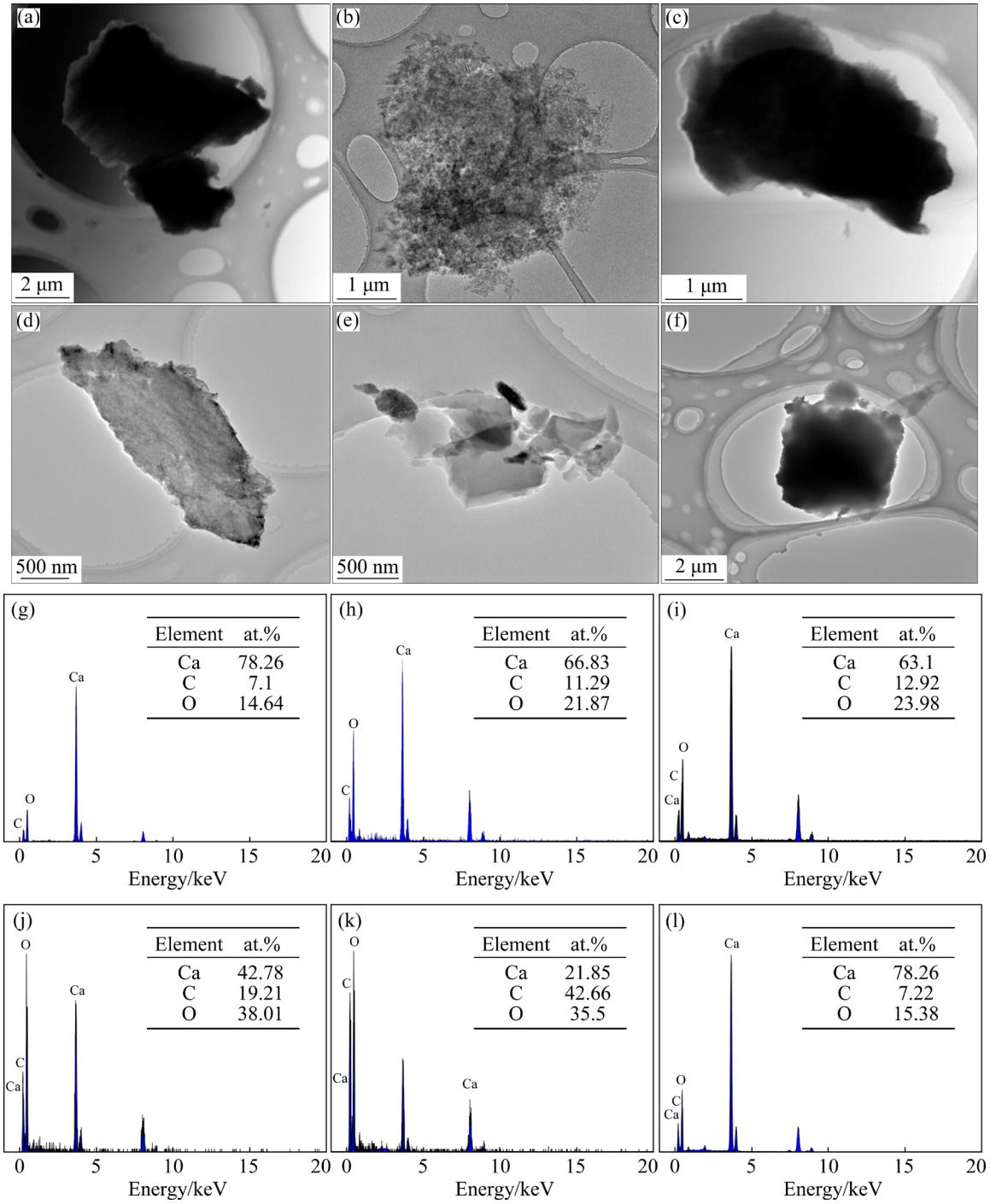

Fig. 6 Effects of monosaccharides and protein on elemental distribution of $CaCO_3$ crystals: (a, g) Control group; (b, h) Glucose; (c, i) Mannose; (d, j) Glucuronic acid; (e, k) Mixed monosaccharides (glucose, mannose and glucuronic acid); (f, l) Catalase

crystals in the groups treated with monosaccharide and control group are still dominated by calcite with a single crystal structure, and most of the (104) crystal faces of calcite are clearly visible (Figs. 7(g–j)). The polycrystalline rings appear as the vaterite content increases in the presence of mixed monosaccharides (Fig. 7(l)).

3.4 Discussion

3.4.1 Effects of monosaccharides on crystalline phases and morphology of $CaCO_3$ crystals

Previous studies have investigated the role of EPS produced by bacteria in the formation of $CaCO_3$ crystals [19,34]. In this study, we found that the monosaccharides have the capacity to alter both

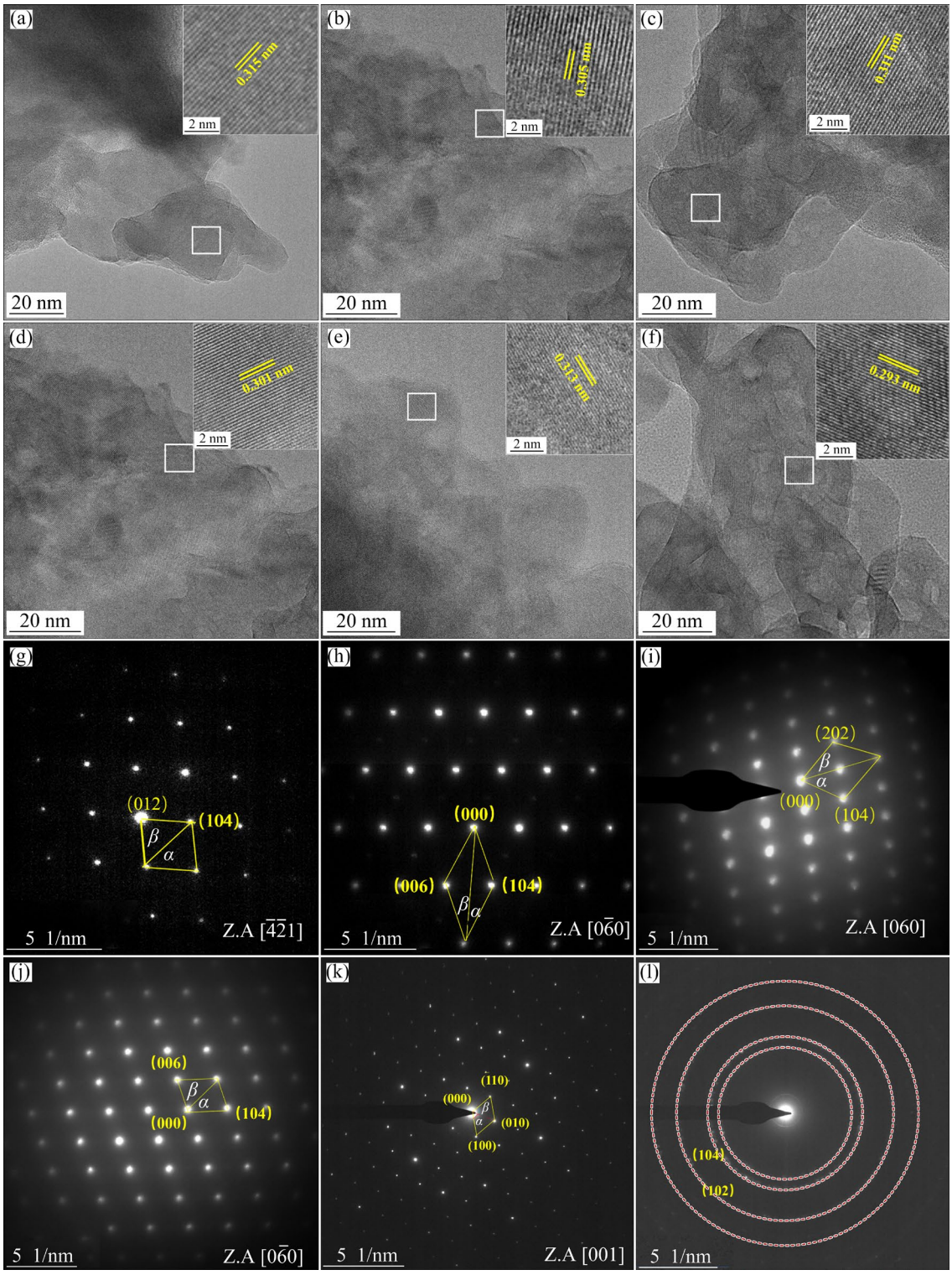

Fig. 7 Lattice spacing and electron diffraction of $CaCO_3$ crystals in the presence of monosaccharides and protein: (a, g) Control group; (b, h) Glucose; (c, i) Mannose; (d, j) Glucuronic acid; (e, k); Catalase; (f, l) Mixed monosaccharides (glucose, mannose and glucuronic acid)

the crystalline phases and morphology of $CaCO_3$ crystals. Also, our observations are consistent with previous studies. For example, TOURNEY and NGWENYA [34] found that the EPS can inhibit the growth of vaterite while enhancing the formation of calcite crystals. LIU et al [35], concluded that the resulting crystals are exclusively calcite. Certainly, the crystalline forms of $CaCO_3$ crystals

are affected by a variety of factors, such as pH, Ca^{2+} concentration, temperature, and reaction time [36−38]. LIU et al [35] speculated that the ability of monosaccharides can convert vaterite to calcite, which could be attributed to the electrostatic interaction between functional groups and Ca^{2+} ions, and the geometric matching between functional groups and $CaCO_3$ crystals. Meanwhile, they speculated that Ca^{2+} chelates with —OH and —COOH in monosaccharide molecules through electrostatic interactions, thereby contributing to the formation of calcite. This significant complexation of Ca^{2+} has been unequivocally demonstrated by BRAISSANT et al [8]. Furthermore, $CaCO_3$ crystals induced by glucose and mannose appear to promote the conversion of vaterite to calcite, potentially due to the combination of glucose and mannose with calcium ions through multiple hydroxyl groups [19]. Nevertheless, there are differences between the effects of glucose and mannose on the conversion of vaterite to calcite, due to the isomeric relationship between glucose and mannose. This suggests that the spatial structure of functional groups may play a crucial role while the monosaccharides with the same functional group may not have the same effect on promoting the crystalline forms of $CaCO_3$ crystals. The findings were consistent with the observations of LANG et al [39], who showed that the primary structure of the saccharide molecule, the functional side-groups, orientation of the glycosidic bond, and the degree of branching all could affect the nucleation rate and growth of $CaCO_3$ crystals. Besides, increasing the concentration of monosaccharides could increase the proportion of vaterite within the $CaCO_3$ crystals, indicating that the crystalline phases of $CaCO_3$ crystals might be related to the concentration of monosaccharides. Furthermore, we found that increasing monosaccharides concentration decreased the $CaCO_3$ crystal size, which might be due to the following two reasons: (1) The increased concentration of monosaccharides promoted frequent nucleation, resulting in the formation of more crystals with a smaller size [40,41]; (2) More suitable carbon sources were provided to the bacteria with the increase of monosaccharides concentration. This rise in EPS content, along with an increase in nucleation sites of $CaCO_3$ crystals, contributes to the reduction in crystal size.

3.4.2 Effects of protein on crystalline phases and morphology of $CaCO_3$ crystals

Previous studies have investigated the effects of proteins on $CaCO_3$ crystals, revealing that purified eggshell proteins promote the formation of calcite crystals [42]. HONG et al [43] identified fetuin A, osteopontin, and otoconin 90 as potent inhibitors of calcite growth. In our experiments, we found that catalase contributed to the regular morphology of $CaCO_3$ crystals without impacting the crystalline phase conversion. From here, we infer that catalase could stabilize certain crystal planes by adhering on the surface of the crystals. This observation is consistent with prior studies that have shown that some proteins can interact with several crystal planes [19]. As for the role of proteins in the crystalline phases of $CaCO_3$ crystals, FEOKTISTOVA et al [25] also confirmed that catalase did not affect the crystalline phases of $CaCO_3$ crystals. In this work, our results further explain the role of catalase, showing that it promotes the agglomeration of spherical particles of $CaCO_3$ crystals. This aggregation could be explained by electrostatic interactions from the van der Waals force [25]. Moreover, previous study showed that mutual adsorption occurred between benzene rings and $CaCO_3$ crystals [44], suggesting an interaction between protein and the crystal surface. In conclusion, our study found that monosaccharides and proteins have different effects on both the crystalline phase conversion and the morphology of $CaCO_3$ crystals.

4 Conclusions

(1) A strain of *K. aerogenes* using calcium acetate as calcium source for $CaCO_3$ mineralization is screened, and the mass of $CaCO_3$ crystals is significantly influenced by the initial pH and calcium acetate concentration.

(2) Additional glucose, mannose, and glucuronic acid produced by *K. aerogenes* can enhance the crystalline form conversion of $CaCO_3$ crystals to calcite and expansion of their sizes. Specifically, the addition of glucuronic acid enhances the crystalline form conversion of $CaCO_3$ crystals to rhombic calcite completely and improves the thermodynamic stability of $CaCO_3$ crystals. In addition, the catalase is beneficial to form $CaCO_3$ crystals with a regular shape and could increase the

size of $CaCO_3$ crystals.

(3) This study provides a theoretical basis for enhancing the crystalline form conversion of $CaCO_3$ crystals by additional monosaccharides and protein in the EPS produced by microbe. This could lead to an improvement in the thermodynamic stability of $CaCO_3$ crystals in the solidified samples for dealing with uranium pollution repository by MICP.

CRediT authorship contribution statement

Nan HU: Conceptualization, Methodology, Project administration, Writing − Review & editing; **Ai-shu LI:** Methodology, Investigation, Data curation, Writing − Review & editing; **Huang YU:** Writing − Review & editing; **Yu-long LIU:** Investigation, Data curation; **Hui ZHANG:** Resources, Supervision; **Zhi-hui YANG:** Project administration, Funding acquisition; **Guang-yue LI:** Project administration, Supervision; **De-xin DING:** Conceptualization, Writing − Review & editing, Supervision.

Declaration of competing interest

The authors declare that they have no known competing financial interests or personal relationships that could have appeared to influence the work reported in this paper.

Acknowledgments

This work was supported by the National Natural Science Foundation of China (Nos. U20A20267, U1967210, 12275123), Hunan Provincial Science Fund for Distinguished Young Scholars, China (No. 2022JJ10041), and the Program of Science and Technology Department of Hunan Province, China (Nos. 2020 TJ-Q03, 2022SK2077).

Supporting information

Supporting information in this paper can be found at: http://tnmsc.csu.edu.cn/download/20-p4085-2023-1373-Supporting_Information.pdf.

References

[1] REN Zheng, ZHANG Si-qin, SHU Yang-zhen, FU Xi-biao, PENG Guo-wen. Preparation of new function material MIL-125-NH-PO and its adsorption capability for U(VI) [J]. The Chinese Journal of Nonferrous Metals, 2022, 32(11): 3406−3418. (in Chinese)

[2] DING De-xin, TAN Guo-chi, ZHANG Qi, TAO De-min, ZHANG Hui, LI Guang-yue, HU Nan. Enhancement effects of weak electric field on uranium and manganese removal from leachate of uranium tailings impoundment by artificial wetland [J]. Journal of Cleaner Production, 2022, 363: 132601.

[3] HU Nan, LIU Jing-jing, MA Jian-hong, ZHANG Qi, ZHANG Hui, DAI Zhong-ran, DING De-xin. Remediation of groundwater in decommissioned mining area of acid in-situ leaching uranium mine by microbial community [J]. The Chinese Journal of Nonferrous Metals, 2023, 33(6): 2031−2042. (in Chinese)

[4] SONG Meng-zhu, JU Tong-yao, MENG Yuan, HAN Si-yu, LIN Li, JIANG Jian-guo. A review on the applications of microbially induced calcium carbonate precipitation in solid waste treatment and soil remediation [J]. Chemosphere, 2022, 290: 133229.

[5] FUJITA Y, FERRIS F G, LAWSON R D, COLWELL F S, SMITH R W. Subscribed content calcium carbonate precipitation by ureolytic subsurface bacteria [J]. Geomicrobiology Journal, 2000, 17(4): 305−318.

[6] DUPRAZ C, VISSCHER P T, BAUMGARTNER L K, REID R P. Microbe-mineral interactions: Early carbonate precipitation in a hypersaline lake (Eleuthera Island, Bahamas) [J]. Sedimentology, 2004, 51(4): 745−765.

[7] van PAASSEN L A, DAZA C M, STAAL M, SOROKIN D Y, van der ZON W, van LOOSDRECHT M C M. Potential soil reinforcement by biological denitrification [J]. Ecological Engineering, 2010, 36(2): 168−175.

[8] BRAISSANT O, DECHO A W, DUPRAZ C, GLUNK C, PRZEKOP K M, VISSCHER P T. Exopolymeric substances of sulfate-reducing bacteria: Interactions with calcium at alkaline pH and implication for formation of carbonate minerals [J]. Geobiology, 2007, 5(4): 401−411.

[9] GAT D, RONEN Z, TSESARSKY M. Long-term sustainability of microbial-induced $CaCO_3$ precipitation in aqueous media [J]. Chemosphere, 2017, 184: 524−531.

[10] BU Chang-ming, LU Xin-yu, ZHU Dong-xu, LIU Lei, SUN Yi, WU Qiu-tong, ZHANG Wen-tao, WEI Qi-ke. Soil improvement by microbially induced calcite precipitation (MICP): A review about mineralization mechanism, factors, and soil properties [J]. Arabian Journal of Geosciences, 2022, 15(9): 863.

[11] ABDEL-BASSET R, HASSAN E A, GROSSART H P. Manifestations and environmental implications of microbially-induced calcium carbonate precipitation (MICP) by the cyanobacterium *Dolichospermum flosaquae* [J]. Biogeosciences, 2020, 17: 1−20.

[12] BUCCI P, COPPOTELLI B, MORELLI I, ZARITZKY N, CARAVELLI A. Micronutrients and COD/N ratio as factors influencing granular size and SND in aerobic granular sequencing batch reactors operated at low organic loading [J]. Journal of Water Process Engineering, 2022, 46: 102625.

[13] XIANG Jun-cheng, QIU Jing-ping, WANG Yu-guang, GU Xiao-wei. Calcium acetate as calcium source used to biocement for improving performance and reducing ammonia emission [J]. Journal of Cleaner Production, 2022, 348: 131286.

[14] WEI Yan, XU Hao, XU Shuang-meng, SU Hui, SUN Rui-ze, HUANG Di, ZHAO Li-qin, HU Yin-chun, WANG Kai-qun, LIAN Xiao-jie. Synthesis and characterization of calcium carbonate on three kinds of microbial cells templates [J]. Journal of Crystal Growth, 2020, 547: 125755.

[15] DRAKE J L, BENAYAHU Y, POLISHCHUK I, POKROY B, PINKAS I, MASS T. Sclerites of the soft coral *Ovabunda macrospiculata* (Xeniidae) are predominantly the metastable $CaCO_3$ polymorph vaterite [J]. Acta Biomaterialia, 2021, 135: 663−670.

[16] GU Zhao-rui, CHEN Qing, WANG Li-shuang, NIU Shuang, ZHENG Jun-jie, YANG Min, YAN Yun-jun. Morphological changes of calcium carbonate and mechanical properties of samples during microbially induced carbonate precipitation (MICP) [J]. Materials, 2022, 15(21): 7754.

[17] WU Jun, ZENG R J. Biomimetic regulation of microbially induced calcium carbonate precipitation involving immobilization of *Sporasarcina pasteurii* by sodium alginate [J]. Crystal Growth & Design, 2017, 17(4): 1854−1862.

[18] KAYANO K, SARUWATARI K, KOGURE T, SHIRAIWA Y. Effect of coccolith polysaccharides isolated from the coccolithophorid, emiliania huxleyi, on calcite crystal formation in vitro $CaCO_3$ crystallization [J]. Marine Biotechnology, 2011, 13: 83−92.

[19] AZULAY D N, ABBASI R, BEN SIMHON KTORZA I, REMENNIK S, REDDY M A, CHAI L. Biopolymers from a bacterial extracellular matrix affect the morphology and structure of calcium carbonate crystals [J]. Crystal Growth & Design, 2018, 18(9): 5582−5591.

[20] NAGAOKA H, NEMOTO H. Influence of extracellular polymeric substances on nitrogen removal in an intermittently-aerated membrane bioreactor [J]. Water Science and Technology, 2005, 51(11): 151−158.

[21] LONG Guo-yu, ZHU Ping-ting, SHEN Yun, TONG Mei-ping. Influence of extracellular polymeric substances (EPS) on deposition kinetics of bacteria [J]. Environmental Science & Technology, 2009, 43(7): 2308−2314.

[22] DEMIR R, ŞAHAR U, DEVECI R. Determination of terminal glycan and total monosaccharide profiles of reelin glycoprotein in SH-SY5Y neuroblastoma cell line by lectin blotting and capillary liquid chromatography electrospray ionization-ion trap tandem mass spectrometry system [J]. Biochimica et Biophysica−Proteins and Proteomics, 2021, 1869(2): 140559.

[23] WANG Ning, WU Xiao-lin, KU Li-xia, CHEN Yan-hui, WANG Wei. Evaluation of three protein-extraction methods for proteome analysis of maize leaf midrib, a compound tissue rich in sclerenchyma cells [J]. Frontiers in Plant Science, 2016, 7: 856.

[24] ZHENG Tian-wen, QIAN Chun-xiang. Influencing factors and formation mechanism of $CaCO_3$ precipitation induced by microbial carbonic anhydrase [J]. Process Biochemistry, 2020, 91: 271−281.

[25] FEOKTISTOVA N A, VIKULINA A S, BALABUSHEVICH N G, SKIRTACH A G, VOLODKIN D. Bioactivity of catalase loaded into vaterite $CaCO_3$ crystals via adsorption and co-synthesis [J]. Materials & Design, 2020, 185: 108223.

[26] VIKULINA A S, FEOKTISTOVA N A, BALABUSHEVICH N G, SKIRTACH A G, VOLODKIN D. The mechanism of catalase loading into porous vaterite $CaCO_3$ crystals by co-synthesis [J]. Physical Chemistry Chemical Physics, 2018, 20(13): 8822−8831.

[27] CHENG Meng, SUN Sheng-tong, WU Pei-yi. Microdynamic changes of moisture-induced crystallization of amorphous calcium carbonate revealed via in situ FTIR spectroscopy [J]. Physical Chemistry Chemical Physics, 2019, 21(39): 21882−21889.

[28] BENIASH E, AIZENBERG J, ADDADI L, WEINER S. Amorphous calcium carbonate transforms into calcite during sea urchin larval spicule growth [J]. Proc Biol Sci, 1997, 264(1380): 461−465.

[29] OLIVEIRA R C, HAMMER P, GUIBAL E, TAULEMESSE J M, GARCIA O. Characterization of metal-biomass interactions in the lanthanum (III) biosorption on *Sargassum* sp. using SEM/EDX, FTIR, and XPS: Preliminary Studies [J]. Chemical Engineering Journal, 2014, 239: 381−391.

[30] QIAN Xin-yi, FANG Chao-lin, HUANG Min-sheng, ACHAL V. Characterization of fungal-mediated carbonate precipitation in the biomineralization of chromate and lead from an aqueous solution and soil [J]. Journal of Cleaner Production, 2017, 164: 198−208.

[31] TANAKA M, OGASAWARA S. Infrared study of adsorbed state of aniline on alumina and HCl-treated alumina [J]. Journal of Catalysis, 1972, 25(1): 111−117.

[32] BAI Hui, LIU Deng, ZHENG Wei-li, MA Li-yuan, YANG Shan-shan, CAO Jin-peng, LU Xiao-lu, WANG Hong-mei, MEHTA N. Microbially-induced calcium carbonate precipitation by a halophilic ureolytic bacterium and its potential for remediation of heavy metal-contaminated saline environments [J]. International Biodeterioration & Biodegradation, 2021, 165: 105311.

[33] LYU Jie-jie, LI Fu-chun, ZHANG Chong-hong, GOWER L, WASMAN S, SUN Jun, YANG Guo-guo, CHEN Jia-ni, GU Li-xin, TANG Xu, SCHEIFFELE G. From the inside out: Elemental compositions and mineral phases provide insights into bacterial calcification [J]. Chemical Geology, 2021, 559: 119974.

[34] TOURNEY J, NGWENYA B T. Bacterial extracellular polymeric substances (EPS) mediate $CaCO_3$ morphology and polymorphism [J]. Chemical Geology, 2009, 262(3/4): 138−146.

[35] LIU Shuang, WU Hao, LU Xiang, QU Jin-ping. Regulation of calcium carbonate biomimetic mineralization by biomass polysaccharide with different molecular weights and spatial configurations [J]. ES Food and Agroforestry, 2022, 9: 45−53.

[36] ÇAĞATAY M O, BATUR E. Influence of pH on morphology, size and polymorph of room temperature synthesized calcium carbonate particles [J]. Powder Technology, 2018, 339: 781−788.

[37] LI Wei, CHEN Wei-shan, ZHOU Peng-peng, ZHU Shi-lin, YU Long-jiang. Influence of initial calcium ion concentration on the precipitation and crystal morphology of calcium carbonate induced by bacterial carbonic anhydrase [J]. Chemical Engineering Journal, 2013, 218: 65−72.

[38] SOVOVA S, ABALYMOV A, PEKAR M, SKIRTACH A G, PARAKHONSKIY B. Calcium carbonate particles: Synthesis, temperature and time influence on the size, shape, phase, and their impact on cell hydroxyapatite formation [J]. Journal of Materials Chemistry B, 2021, 9(39): 8308−8320.

[39] LANG A, MIJOWSKA S, POLISHCHUK I, FERMANI S, FALINI G, KATSMAN A, MARIN F, POKROY B. Acidic monosaccharides become incorporated into calcite single

crystals [J]. Chemistry European, 2020, 26(70): 16860−16868.
[40] WALKER J M, MARZEC B, LEE R, VODRAZKOVA K, DAY S J, TANG C C, RICKABY R E M, NUDELMAN F. Polymorph selectivity of coccolith-associated polysaccharides from *Gephyrocapsa oceanica* on calcium carbonate formation in vitro [J]. Advanced Functional Materials, 2019, 29(1): 1807168.
[41] REHMAN S, ASIRI S M, KHAN F A, JERMY B R, RAVINAYAGAM V, ALSALEM Z, AL JINDAN R, QURASHI A. Anticandidal and in vitro anti-proliferative activity of sonochemically synthesized indium tin oxide nanoparticles [J]. Scientific Reports, 2020, 10(1): 3228.
[42] HERNÁNDEZ-HERNÁNDEZ A, VIDAL M L, GÓMEZ-MORALES J, RODRÍGUEZ-NAVARRO A B, LABAS V, GAUTRON J, NYS Y, GARCÍA RUIZ J M. Influence of eggshell matrix proteins on the precipitation of calcium carbonate ($CaCO_3$) [J]. Journal of Crystal Growth, 2008, 310(7/8/9): 1754−1759.
[43] HONG Mi-na, MORELAND K T, CHEN Jia-jun, TENG H H, THALMANN R, de YORED J J. Effect of otoconial proteins fetuin A, osteopontin, and otoconin 90 on the nucleation and growth of calcite [J]. Crystal Growth & Design, 2015, 15(1): 129−136.
[44] KIM S, MARCANO M C, BECKER U. Mechanistic study of wettability changes on calcite by molecules containing a polar hydroxyl functional group and nonpolar benzene rings [J]. Langmuir, 2019, 35(7): 2527−2537.

产气克雷伯氏杆菌胞外聚合物中的单糖和蛋白质对碳酸钙晶型的影响

胡 南[1]，李艾书[1,2]，余 黄[1]，刘玉龙[1]，张 辉[1]，杨志辉[2]，李广悦[1]，丁德馨[1]

1. 南华大学 铀矿冶生物技术国防重点学科实验室，衡阳 421001；
2. 中南大学 冶金与环境学院，长沙 410083

摘 要：筛选一株可以分解乙酸钙形成 $CaCO_3$ 沉淀的菌株—产气克雷伯氏杆菌，确定其诱导产生 $CaCO_3$ 沉淀产量的最适条件为 0.25 mol/L 乙酸钙、4%接种量及 pH 7，随后，分析产气克雷伯氏杆菌胞外聚合物中的单糖和蛋白质成分，研究单糖和蛋白质对 $CaCO_3$ 晶型转化的影响，发现添加单糖能促进 $CaCO_3$ 晶相从球霰石向方解石转变。其中，添加 1.00 g/L 葡萄糖醛酸可促使 $CaCO_3$ 晶体在 5 d 后完全转变为方解石。同时，添加过氧化氢酶能使 $CaCO_3$ 晶体的形貌更加规则，但对晶相没有影响。结果表明，加入葡萄糖醛酸对 $CaCO_3$ 晶体的晶型有显著影响。

关键词：铀；$CaCO_3$ 晶体；微生物诱导 $CaCO_3$ 沉淀；胞外聚合物；产气克雷伯氏杆菌

(Edited by Xiang-qun LI)